

Population study for γ -ray emitting Millisecond Pulsars and *Fermi* unidentified sources

J. Takata, Y. Wang, K.S. Cheng

Department of Physics, University of Hong Kong, Pokfulam Road, Hong Kong

The *Fermi*-LAT has revealed that rotation powered millisecond pulsars (MSPs) are a major contributor to the Galactic γ -ray source population. We discuss the γ -ray emission process within the context of the outer gap accelerator model, and use a Monte-Carlo method to simulate the Galactic population of the γ -ray emitting MSPs. We find that the outer gap accelerator controlled by the magnetic pair-creation process is preferable in explaining the possible correlation between the γ -ray luminosity and the spin down power. Our Monte-Carlo simulation implies that most of the γ -ray emitting MSPs are radio quiet in the present sensitivity of the radio survey, indicating that most of the γ -ray MSPs have been unidentified. We argue that the Galactic *Fermi* unidentified sources located at high latitudes should be dominated by MSPs, whereas the sources in the galactic plane are dominated by radio-quiet canonical pulsars.

1. Introduction

The *Fermi* Large Area Telescope (*Fermi*-LAT) has discovered over 80 γ -ray pulsars, and revealed that the γ -ray pulsars are a major class of Galactic γ -ray sources. Of these, *Fermi*-LAT first detected pulsed γ -ray emission from 11 millisecond pulsars (Abdo et al. 2010a, 2009a,b; Saz Parkinson et al. 2010; Guillemot et al. 2011). Furthermore, the detection of radio millisecond pulsars (MSPs) associated with over 20 unidentified *Fermi* point sources (e.g. Ransom et al. 2011; Keith et al. 2011) has been reported, suggesting that the millisecond pulsar, as well as the canonical pulsar is one of the major Galactic γ -ray source. The γ -ray emission from pulsars have been discussed in the context of a polar cap accelerator (Ruderman & Sutherland 1975), a slot gap (Harding & Muslimov 2011) and an outer gap accelerator (Cheng, Ho & Ruderman 1986; Takata, Wang & Cheng 2010b).

The high quality data measured by the *Fermi* enable us to perform a detail study for population of the γ -ray pulsars. For example, Takata et al. (2010b) and Takata, Wang and Cheng (2011d) have studied the possible relation between the high-energy emission properties and pulsar spin down power in the context of the outer gap accelerator model. They proposed that the outer gap accelerator model controlled by the magnetic pair-creation process can explain the observed population statistics better than that controlled by the photon-photon pair-creation process (e.g. Zhang & Cheng 2003). Story, Gonthier & Harding (2007) studied the population of γ -ray millisecond pulsars within the context of the slot gap accelerator model, and predicted the *Fermi* observations. They predicted that the *Fermi* will detect 12 radio-loud and 33-40 radio-quiet γ -ray millisecond pulsars. With the Monte-Carlo simulation of the outer gap, Takata, Wang & Cheng (2011a,b) have explained the observed distributions of the characteristics of the γ -ray pulsars detected by the *Fermi* with the six-month long observation. The population studies (e.g. Kaaret &

Philip 1996; Takata et al. 2011b,c) have also pointed out that unidentified MSPs located at high-Galactic latitudes will associate with the *Fermi* unidentified sources (Abdo et al. 2010b).

In this proceeding, we will review our recent Monte-Carlo studies for the Galactic population of the γ -ray emitting MSPs (Takata et al. 2010b; Takata et al. 2011a,b,c) and the possible association with the *Fermi* unidentified sources.

2. γ -ray emission from outer gap

2.1. γ -ray luminosity

For the outer gap model, the luminosity of the γ -ray emissions is typically

$$L_\gamma \sim f^3 L_{sd}, \quad (1)$$

where L_{sd} is the spin down power of the pulsar and the gap fraction f is defined as the ratio of the gap thickness at the light cylinder to the light cylinder radius $R_{lc} = Pc/2\pi$, where P is pulsar rotation period.

Zhang & Cheng (2003) have argued a self-consistent outer gap model controlled by the photon-photon pair-creation process between the curvature photons and the X-rays from the stellar surface. They estimated the gap fraction for the MSPs as

$$f_p = 7.0 \times 10^{-2} (P/1 \text{ ms})^{26/21} (B_s/10^8 \text{ G})^{-4/7} \delta r_5^{2/7}, \quad (2)$$

where B_s is the stellar magnetic field of the global dipole field and δr_5 is the distance (in units of 10^5 cm) from the stellar surface to the position, where the local multiple magnetic field, which dominates the global dipole field, is comparable to the dipole field, and it will be $\delta r_5 \sim 1 - 10$ cm.

Takata et al. (2010b) argued that the incoming particles emit photons with an energy $m_e c^2 / \alpha_f \sim 70 \text{ MeV}$ by curvature radiation near the stellar surface and

that these photons can become pairs via the magnetic pair creation process. For a simple dipole field structure, all pairs move inward and cannot affect the outer gap accelerator. However if the local field lines near the surface are bent sideward due to the strong multipole field, the pairs created in these local magnetic field lines can have an angle greater than 90° , which results in an outgoing flow of pairs. In this model, the fractional gap thickness in this circumstance is

$$f_m \sim 0.025 K P_{-3}^{1/2}, \quad (3)$$

where $K \sim B_{m,12}^{-2} s_7$ characterizes the local parameters. Here, $B_{m,12}$ and s_7 are the strength of the local magnetic field in units of 10^{12} G and the local curvature radius in units of 10^7 cm, respectively, near the stellar surface.

The γ -ray luminosity L_γ (1) can be cast in terms of the spin down power $L_{sd} = 2(2\pi)^4 \mu / (3c^3 P^4)$ as

$$L_\gamma^p \sim 10^{32} L_{sd,34}^{1/14} B_8^{1/7} \delta_5^{6/7} \text{ erg s}^{-1}, \quad (4)$$

for the outer gap controlled by the photon-photon pair-creation process, and

$$L_\gamma^m \sim 6 \times 10^{32} L_{sd,34}^{5/8} K_1^3 B_8^{3/4} \text{ erg s}^{-1}, \quad (5)$$

by the magnetic pair-creation process. Here, $L_{sd,34} = (L_{sd}/10^{34} \text{ erg s}^{-1})$, $K_1 = K/10$ and $B_8 = B_s/10^8 \text{ G}$.

In Figures 1 the model predictions given by equations (4) and (5) are plotted with the solid line or dashed line, respectively. The filled circles represent the MSPs detected by the *Fermi*-LAT. Notwithstanding the large observational errors, the data points at large L_γ in Figures 1 may suggest that the magnetic pair-creation model for the gap closing process is preferred over the photon-photon pair-creation model for the $L_\gamma - L_{sd}$ relation.

2.2. Two layer outer gap model

A simple description of the electric field structure inside the two-layer outer gap is discussed in Wang, Takata & Cheng (2010). We illustrate the picture for the gap structure in Figure 2, where we denote z as the coordinate perpendicular to the magnetic field line in the poloidal plane, and ρ is the charge density. In the main acceleration region, the charge density is $\sim 10\%$ of the Goldreich-Julian value, and an electric field along the magnetic field line accelerates the electrons and positrons up to the Lorentz factor of $\Gamma \sim 10^{7.5}$ and the accelerated particles emit $\sim \text{GeV}$ photons via the curvature radiation process. In the screening region, the large number of pairs created by the pair-creation process starts to screen out the gap electric field.

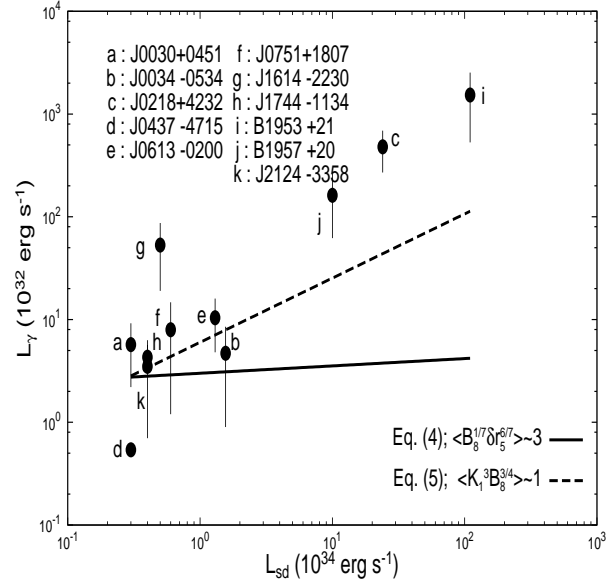


Figure 1: The γ -ray luminosity and the spin down power for the MSPs. The sole and dashed line are the relation predicted by the outer gap model controlled by the photon-photon pair-creation process and by the magnetic pair-creation process, respectively. The observed luminosity is $L_\gamma = 4\pi d^2 F$ with d being the distance and F the observed flux. See Takata et al. 2011d.

2.2.1. Charge density distribution

The previous electrodynamics studies expect that the particle number density increases exponentially near the boundary ($z = h_1$) between the main acceleration and screening regions (Cheng et al. 1986), we approximately describe the distribution of the charge density in the z -direction as follows (Fig. 2)

$$\rho(\vec{r}) = \begin{cases} \rho_1(x, \phi), & \text{if } 0 \leq z \leq h_1(x, \phi), \\ \rho_2(x, \phi), & \text{if } h_1(x, \phi) < z \leq h_2(x, \phi), \end{cases} \quad (6)$$

where x and ϕ represent the coordinates along the magnetic field and the azimuthal direction. In addition, $z = 0$ and $z = h_2$ correspond to the last-open field line and the upper boundary of the gap, respectively. For simplicity, we assume that the upper boundary (h_2) as well as the boundary (h_1) is defined with a given magnetic field line. Because the charge density in the screening region will be proportional to the Goldreich-Julian charge density, we approximate that $\rho - \rho_{GJ} \sim g(z, \phi) \rho_{GJ}(\vec{r})$, where

$$g(z, \phi) = \begin{cases} -g_1(\phi), & \text{if } 0 \leq z \leq h_1(x, \phi), \\ g_2(\phi), & \text{if } h_1(x, \phi) < z \leq h_2(x, \phi). \end{cases} \quad (7)$$

and $g_1 > 0$ and $g_2 > 0$ so that $|\rho| < |\rho_{GJ}|$ for the main acceleration region and $|\rho| > |\rho_{GJ}|$ for the screening region. In this paper, by neglecting the z -dependence of the Goldreich-Julian charge density, we approximate as $\rho_{GJ}(x, \phi) \sim -\Omega B x / 2\pi c R_c$, where Ω and R_c

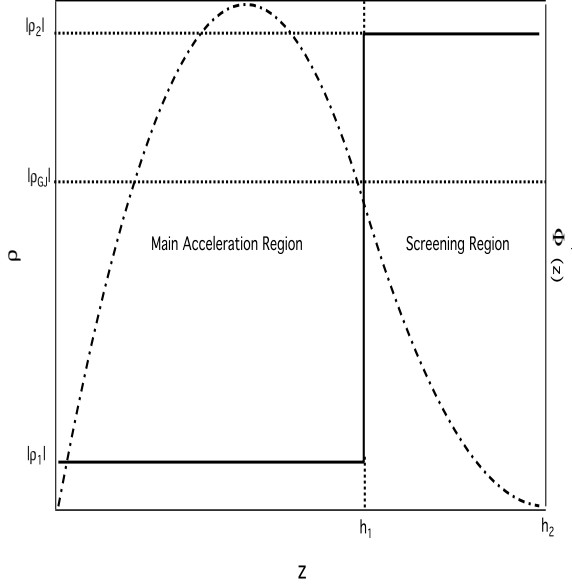


Figure 2: The simplified distribution of the charge density (solid line) and the corresponding accelerating potential (dotted line) of the two-layer outer gap. See Wang et al. 2011.

are the angular frequency of the pulsar and the curvature radius of the field line, respectively.

2.2.2. Accelerating electric field

To obtain the typical strength of the electric field in the gap, we find the solution of the Poisson equation for each azimuthal angle (Wang et al. 2010),

$$\frac{\partial^2}{\partial z^2} \Phi'(x, z, \phi)|_{\phi=\text{fixed}} = -4\pi[\rho(x, z, \phi) - \rho_{GJ}(\vec{r})]|_{\phi=\text{fixed}}, \quad (8)$$

where Φ' is the electric potential of the accelerating field. The boundary conditions on the lower ($z = 0$) and upper ($z = h_2$) boundaries are given by $\Phi'(x, z = 0, \phi) = \Phi'(x, z = h_2, \phi) = 0$. Imposing Φ' and $\partial\Phi'/\partial z$ are continuous at the boundary $z = h_1$, we eventually obtain the solution of the accelerating electric field ($E_{||} = -\partial\Phi'/\partial x$) as

$$E_{||}(\vec{r}) \sim \frac{\Omega B h_2^2(x, \phi)}{c R_s} [-g_1(\phi) z'^2 + C_1(\vec{r}) z'], \quad (9)$$

for $0 \leq z' \leq h_1/h_2$ and

$$E_{||}(\vec{r}) \sim \frac{\Omega B h_2^2(x, \phi)}{c R_s} [g_2(\phi)(z'^2 - 1) + D_1(\vec{r})(z' - 1)] \quad (10)$$

for $h_1/h_2 < z' \leq 1$, where $z' = z/h_2$,

$$C_1(x, \phi) = -[g_1 h_1 (h_1 - 2h_2) + g_2 (h_1 - h_2)^2]/h_2^2,$$

and

$$D_2(x, \phi) = -(g_1 h_1^2 + g_2 h_2^2)/h_2^2.$$

In addition, we used the relations of the dipole field that $\partial(Bh_2^2)/\partial x \sim 0$, $\partial z'/\partial x \sim 0$, $\partial(h_1/h_2)/\partial x \sim 0$, and approximated that $\partial R_c/\partial x \sim 0$.

On the upper boundary, the total potential field (co-rotational + non co-rotational potentials) in the gap is continuously connected to the co-rotational potential field outside the gap, giving $\partial\Phi'/\partial z|_{z=h_2} = -E_{\perp}(z = h_2) = 0$, yielding the relation between (h_1, h_2) and (g_1, g_2) as

$$(h_2/h_1)^2 = 1 + (g_1/g_2). \quad (11)$$

The gap thickness h_2 is calculated that $h_2 \sim f R_{lc}$, where f is the fractional gap thickness given by Eq.(2) or Eq. (3). In this paper, we present the results using the ratio of $h_1/h_2 = 0.95$ and the dimensionless charge density of main acceleration region $1 - g_1 = 0.3$ (Takata et al. 2011c). The normalized charge density of the screening region, g_2 is calculated from the equation (11). The Lorentz factor of the accelerated particles is obtained by the force balance between the electric field and the curvature radiation drag force as

$$\Gamma = \left(\frac{3R_c^2}{2e} E_{||} \right)^{1/4}. \quad (12)$$

To examine the dependency of γ -ray emission properties on the viewing geometry, we explore the typical 3-D geometry of the outer gap (Takata et al. 2011c). We calculate the curvature radiation process for each emitting point, at which the curvature photons are emitted in the direction of the particle motion. Figure 3 shows the γ -ray flux (≥ 100 MeV) as a function of the viewing angle ζ and of the inclination angle α . Here we calculated the rotation period from $B_s = 3 \times 10^{12}$ G and the gap fraction $f = f_p = 0.25$. We can see that the calculated flux tends to decrease as the line of sight approaches to the rotation axis, where $\zeta = 0^\circ$. This is because a large viewing angle ($\zeta \rightarrow 90^\circ$) can encounter more intense emission region, whereas the small viewing angle ($\zeta \ll 90^\circ$) will encounter the less intense region or even miss the emission region. Also we find in Figure 3, a larger inclination angle shows a larger observed flux for a smaller Earth viewing angle. These dependences of the γ -ray flux on the viewing geometry implies that the *Fermi* has likely detected a greater number of the pulsars with larger inclination angles and larger viewing angles near 90° .

3. Monte-Carlo simulation

We simulate that Galactic distribution of MSPs using the Monte-Carlo method developed by the previous studies (e.g. Sturmer & Dermer 1996). We would like to remark that for MSPs, the Galactic distribution will not depend on the spin down age

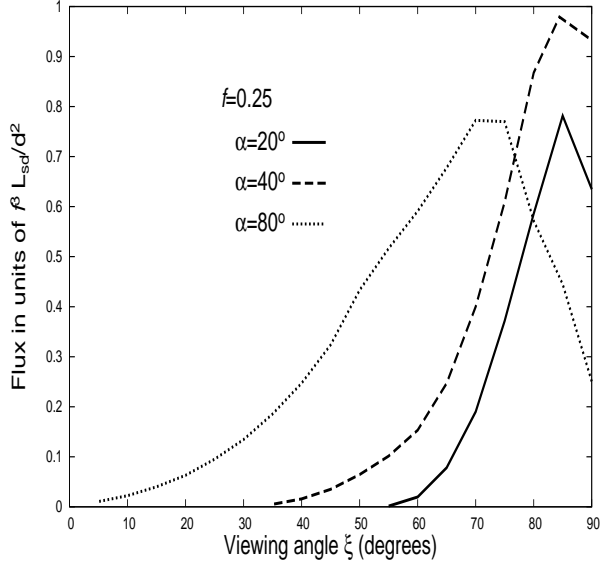


Figure 3: Dependency of the observed γ -ray flux on the viewing angle (ξ) and the inclination angle (α). $f = f_p = 0.25$. See Takata et al. (2011c).

of the MSPs. With the typical velocity of the observed MSPs, $V \sim 70$ km/s, it is expected that the displacement of the MSPs (or binary system) with the typical age, ≥ 100 Myr, becomes larger than the size of the Galaxy. With the relatively slow velocity, $V \leq 100$ km/s, however, the MSPs remain bound in the Galactic potential and hence their Galactic distribution does not depend on the spin down age. Because the independence of the Galactic distribution on the spin down age, we assign the “current” pulsar properties for simulated MSPs; namely, we (1) randomly select the age of the simulated MSP up to 10 Gyr, (2) shifts the simulated MSP from its birth location to the current location, and (3) assign the parameters of the MSP following the observed distributions.

For each simulated MSPs, we assume the radio cone is centered on the magnetic axis with a width described by the model of Kramer & Xilouris (2000). Because the γ -ray flux depends on the viewing geometry (Figure 3), we assume that the viewing angle and the inclination angle are randomly distributed for each simulated MSP.

For the sensitivity of the *Fermi* observations, we refer the sensitivity of *Fermi* the six-month long observations (Abdo et al. 2010b) for the radio selected MSPs. However, there are no detections of the γ -ray-selected MSPs so far, we cannot simulate the *Fermi* sensitivity of the blind search of the MSPs. In this paper, therefore, we simulate the population of the γ -ray-selected MSPs with the *Fermi* sensitivity of the blind search of canonical pulsar. To simulate a longer *Fermi* observation, we scale the sensitivity as $\propto \sqrt{T}$, where T is the length of the observation time.

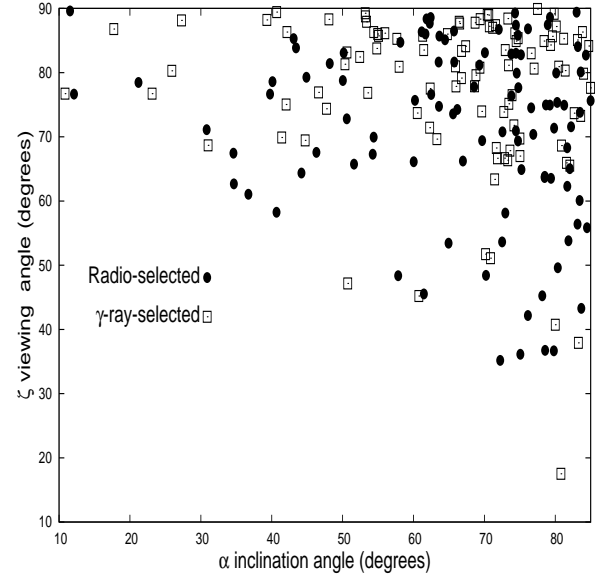


Figure 4: The inclination angle α and the viewing angle ξ for the simulated γ -ray MSPs. Filled circles: Radio selected pulsars. Boxes: γ -ray-selected pulsars. See Takata et al. (2011c).

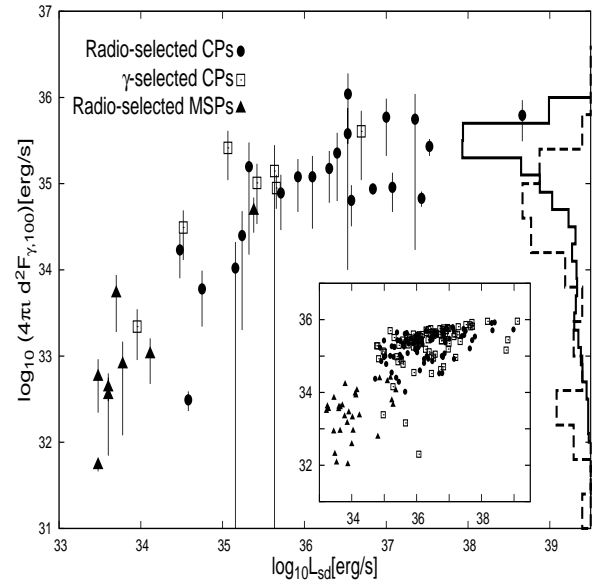


Figure 5: The γ -ray luminosity versus the spin down power for γ -ray emitting MSPs. The 200 samples of the simulated pulsars are plotted in the sub-figure. See Takata et al. (2011c).

4. Results

We present the results of the Monte-Carlo simulation within context of the outer gap model controlled by the magnetic pair-creation process, that is, the fractional gap thickness is given by equation 3.

MSPs	six-months		five-years		ten-years	
	N_r	N_g	N_r	N_g	N_r	N_g
Ra. Sen. (x 1)	10	52	14	200	16	284
Ra. Sen. (x 2)	16	48	26	190	29	274
Ra. Sen. (x 10)	45	32	82	152	94	227
Beaming	106	11	321	41	438	62

Table I Population of simulated radio-selected (N_r) and γ -ray-selected (N_g) MSPs for six-month, five-year and ten-year *Fermi* observations. The first line; the results for ten radio surveys listed in table 1 of Takata et al. (2011a). The second and third lines are the results with the sensitivities increased by a factor of two and ten, respectively, and the bottom is the populations associated with only beaming effects of the radio emission. See Takata et al. 2011c.

4.1. L_γ vs. L_{sd}

Figure 4 plots the distribution of the inclination angle (α) and the viewing angle (ζ) for the simulated γ -ray MSPs. The filled-circles and the boxes represent the radio-selected and γ -ray-selected γ -ray MSPs, respectively. As we can seen in Figure 4, no γ -ray pulsars are detected with a smaller inclination angles and a smaller viewing angles. This is because the γ -ray flux decreases as the viewing angle and/or the inclination angle decrease (c.f. Figure 3). Hence, our simulation result predicts that a greater number of MSPs with larger inclination and larger viewing angles ($\sim 90^\circ$) have been likely detected by the *Fermi* observations.

Figures 5 shows the relation between the γ -ray luminosity and the spin down power. In the figure, we plot the *Fermi* data with errors taken from Abdo et al. (2010a) and Saz Parkinson et al. (2010), and present the simulated 200 pulsars in the sub-figures (except for the γ -ray-selected MSPs). The solid and dashed histograms represent the distributions for the simulated and observed γ -ray pulsars, respectively. The present model predicts that most γ -ray canonical pulsars have a spin down power of $L_{sd} \sim 10^{35-38}$ erg/s and a γ -ray luminosity of $L_\gamma \sim 10^{34-36}$, while MSPs have a $L_{sd} \sim 10^{33-35}$ erg/s and $L_\gamma \sim 10^{32.5-34.5}$ erg/s, which are consistent with the observations.

In Figure 5, we may see that the spin down power L_{sd} and the γ -ray luminosity L_γ of the simulated pulsars can be related as $L_\gamma \propto L_{sd}^\beta$ with $\beta \sim 0$ for $L_{sd} \geq 10^{35-36}$ erg/s and $\beta \sim 0.5$ for $L_{sd} \leq 10^{35-36}$ erg/s. Because the γ -ray luminosity is proportional to $L_\gamma \propto f^3 L_{sd}$ [Eq. (1)], the change of the slope implies the switching gap closure process between the photon-photon pair-creation process, which predicts $L_\gamma \propto L_{sd}^{1/14}$ [Eq. (4)] and the magnetic pair-creation process, which predicts $L_\gamma \propto L_{sd}^{5/8}$ [Eq. (5)].

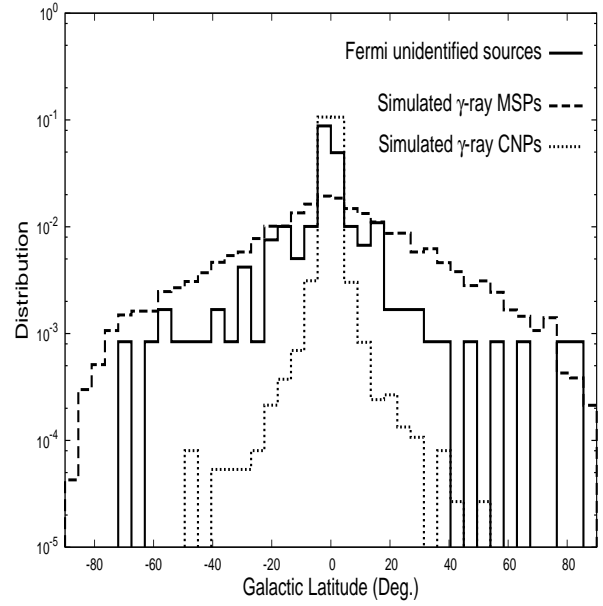


Figure 6: The distributions of Galactic latitudes of the *Fermi* unidentified sources with $V \leq 23.21$ and $C \geq 5$ (solid line), the simulated γ -ray MSPs (dashed line) and canonical pulsars (dotted line). See Takata et al. (2011b).

4.2. Population

In Table 1, we summarize the simulated population of MSPs with the *Fermi* six-month, five-year and ten-year long observations. In addition, the second line (“Ra. Sen. (x2)”) and the third line (“Ra.Sen. (x10)”) in the tables show the results for the radio-surveys increased the sensitivities by a factor of two and of ten, respectively, and the fourth line (“Beaming”) shows the population associated with the only beaming effect of the radio emission.

With the previous radio surveys (first line in Table 1), the present simulation predicts 10 of the radio-selected γ -ray MSPs, which is consistent with the observed number 9 of the *Fermi* six-month long observation. The present model predicts that 14 (or 16) radio-selected γ -ray MSP pulsars will be detected by the *Fermi* with five-year (or ten-year) observations.

We see in the first line of Table 1 that the simulated numbers of radio-selected γ -ray MSPs increase only ~ 10 sources, respectively, over even ten-year *Fermi* observations. This implies that most presently known radio MSPs (~ 80) might not be discovered by the *Fermi* future observations. We also see in Table 1, most simulated γ -ray emitting MSPs are categorized as the γ -ray-selected pulsars with the previous sensitivities of the radio surveys, although the *Fermi* has not confirmed the radio-quiet MSPs. We argue that it may be difficult to identify radio-quiet MSPs, because the detection of the rotation period by the *Fermi* blind search is very difficult due to, for example, the effect orbital motion if the MSP is in binary

system. We expect that the γ -ray-selected MSPs in the simulation correspond to the *Fermi* unidentified sources located at higher Galactic latitudes.

We would like to remark that even we drastically increase the radio sensitivity by a factor of 10, the number of radio-selected MSPs detected by 10 year *Fermi* observations can increase from 16 to 94, which is still much less than the expected 227 γ -ray-selected MSPs. Unless the *Fermi* sensitivity of the blind search is improved, therefore, the most γ -ray MSPs will not be identified and will contribute to the *Fermi* unidentified sources and/or the γ -ray background radiations.

4.3. *Fermi* unidentified sources

In Figure 6, we compare the distributions of the Galactic latitudes for the unidentified *Fermi* sources with the variability index $V \leq 23.21$ and curvature index $C \geq 5$ (solid line, Abdo et al. 2010b), the simulated γ -ray MSPs (dashed line), and canonical pulsars (dotted line) with a flux $F_\gamma \geq 10^{-11}$ erg/cm²s.

We find in Figure 6 that the distribution of the simulated γ -ray MSPs is consistent with that of the *Fermi* unidentified sources. In particular, the MSPs can explain the distribution of the *Fermi* unidentified sources located above the Galactic plane $|b| \geq 10$, which cannot be explained by the canonical γ -ray pulsars, which can mainly explain the unidentified sources located in the Galactic plane. Since the MSPs are in general older than the canonical pulsars, a higher fraction of the γ -ray MSPs, as compared with the canonical pulsars, is located at higher Galactic latitudes. Hence, we expect that γ -ray emitting MSPs are more plausible as the candidate for the origin of the majority of the Galactic *Fermi* unidentified steady sources located in high Galactic latitudes.

Finally, several MSPs in the Black Window (B-W) systems have been discovered at the *Fermi* unidentified sources (Ransom et al. 2011). Because the MSPs in the B-W systems are younger and have higher spin-down power, the γ -ray luminosity will be larger than that of the ordinary MSPs. Furthermore, because the γ -ray emission from the outer gap is stronger in the direction perpendicular to the spin axis, *Fermi* is more likely to discover a greater number of MSPs with the Earth viewing angle $\sim 90^\circ$ measured from the rotation axis (Takata, Cheng & Taam 2010a; Takata et al. 2011c). If the angular momentum transferred from the accreting matter to the neutron star in the accreting stage produces the pulsar's spin axis perpendicular to the orbital plane, the γ -ray emissions from MSPs in B-W system will be stronger on the orbital plane. Hence, the *Fermi* will find the B-W systems with the Earth viewing angle described by edge-on rather than by face-on with respect to the orbital plane. In such a case, a greater number of the *Fermi* Black Window systems show the eclipse of the radio emissions by the

matter ejected from the companion star.

In summary, we have studied the population of the γ -ray emitting MSPs. We find that the observed possible relation between L_γ vs. L_{sd} can be explained by the outer gap model controlled by the magnetic pair-creation process. Our Monte-Carlo study implies that the *Fermi* has detected a greater number of MSPs with larger inclination and larger viewing angles. Furthermore, we expect that most of γ -ray emitting MSPs has been missed by the *Fermi* observations, and still remain as the unidentified sources. It is likely that the Galactic *Fermi* unidentified sources located high galactic latitude are mainly associated with MSPs.

We thank A.H.Kong, C.Y.Hui, P.H.T.Tam, R.H.H.Huang, Lupin-C.C.Lin, M.Ruderman, S.Shibata and R.Taam for the useful discussions. K.S.C. are supported by a GRF grant of Hong Kong Government under HKU700911P.

References

- [1] Abdo A.A. et al. 2010, ApJS, 187, 460
- [2] Abdo A.A. et al., 2010b, ApJS, 188, 405
- [3] Abdo A.A. et al. 2009a, Sci., 325, 840
- [4] Abdo A.A. et al. 2009b, Sci., 325, 848
- [5] Cheng, K. S., Ho, C., & Ruderman, M. 1986, ApJ, 300, 500
- [6] Guillemot, L., et al., 2011, arXiv1110.1271
- [7] Harding, A. K. & Muslimov, A.G. 2011, ApJL, 726, 10
- [8] Kaaret, P., & Cottam, J., 1996, ApJL, 462, 35
- [9] Keith, M.J. et al. 2011, MNRAS, 414, 1292
- [10] Ransom, S.M., et al., 2011, ApJL, 727, 16
- [11] Ruderman M.A., Sutherland P.G. 1975, ApJ, 196, 51
- [12] Saz Parkinson, P.M. et al., 2010, 725, 571
- [13] Story, S.A., Gonthier, P.L., Harding, A.K., 2007, ApJ, 671, 713
- [14] Sturmer, S.J. & Dermer, C.D. 1996 A&AS, 120, 99
- [15] Takata, J., Wang, Y., Cheng, K.S. 2011a, ApJ, 726, 44
- [16] Takata, J., Wang, Y., Cheng, K.S. 2011b, MNRAS, 414, 2173
- [17] Takata, J., Wang, Y., Cheng, K.S. 2011c, MNRAS, 415, 1827
- [18] Takata, J., Cheng, K.S., Taam, R.E. 2011d, submitted
- [19] Takata, J., Cheng, K.S., Taam, R.E. 2010a, ApJL, 723, 68
- [20] Takata, J., Wang, Y., Cheng, K.S. 2010b, ApJ, 715, 1318
- [21] Wang, Y., Takata, J. & Cheng, K.S. 2010, ApJ, 720, 178
- [22] Zhang, L. & Cheng, K.S. 2003, A&A, 398, 639